A&A 400, 347–353 (2003)
DOI: 10.1051/0004-6361:20021844

Astronomy & Astrophysics

Plasma properties above coronal active regions inferred from SOHO/UVCS and radio spectrograph observations

S. Mancuso[1,2], J. C. Raymond[2], J. Kohl[2], Y. -K. Ko[2], M. Uzzo[2], and R. Wu[2]

[1] Istituto Nazionale di Astrofisica (INAF), Osservatorio Astronomico di Torino, Strada Osservatorio 20, Pino Torinese 10025, Italy
[2] Harvard-Smithsonian Center for Astrophysics, 60 Garden Street, MS 50, Cambridge, MA 02138, USA

Received 28 October 2002 / Accepted 13 December 2002

Abstract. Information on coronal plasma was inferred from the joint analysis of type II radio bursts and SOHO UltraViolet Coronagraph Spectrometer (UVCS) observations. The data sample comprises 37 metric type II radio bursts observed by ground-based radio spectrographs in 1999, during the rising phase of the solar cycle. The coronal electron densities n_e were estimated with the diagnostic provided by UVCS observations of the O VI doublet line intensities. Upper limits to the coronal Alfvén speed above active regions were inferred from the derived shock speeds by requiring that the disturbances propagate at least faster than the local characteristic speed. Information on the magnetic field strength B and plasma β in the middle corona were finally extracted from the coronal Alfvén speed upper limits. A major improvement with respect to previous studies that used type II radio bursts to derive plasma properties, is that density profiles of the pre-shock plasma obtained a few hours before the passage of the shock were used instead of general electron density models taken from literature. Our main result is expressed by the inequality $B(r) \leq (0.6 \pm 0.3)(r-1)^{-1.2}$ G, that is valid in the range $1.5 \leq r \leq 2.3$ solar radii, and is consistent with previous estimates of the magnetic field above coronal active regions.

Key words. Sun: corona – Sun: UV radiation – Sun: magnetic fields – Sun: radio radiation – Shock waves

1. Introduction

The difficulty of measuring coronal plasma properties such as the electron density and magnetic field distribution prevents the solution of several open questions in the physics of the solar corona. The combined analysis of radio and extreme ultraviolet spectral signatures can represent a powerful complementary tool to obtain important information about properties of the solar coronal plasma at distances from the Sun that have not been accessed directly by spacecraft. Most of the sources of information on the coronal plasma properties involving radio observations are related to some combination of the magnetic field intensity B and the plasma electron density n_e. Observation of the Faraday rotation of radio signals occulted by the solar corona (Mancuso & Spangler 1999, 2000 and references therein) has been used to infer the plasma structure of the corona through the particular combination $B_{\|}n_e$ found in the definition of rotation measure.

Information on coronal plasma can also be inferred from the analysis of type II radio bursts through the particular combination $B/\sqrt{n_e}$ found in the definition of the Alfvén speed. Type II burst radiation is excited by fast mode MHD shock waves propagating outward through the corona as a result of solar eruptions or blast waves and requires a coherent plasma emission mechanism near the local electron plasma frequency $f_{pe}[\mathrm{Hz}] = 8978\sqrt{n_e[\mathrm{cm}^{-3}]}$ and its second harmonic. This type of burst is associated with slowly drifting (~MHz s^{-1}) and narrow-band (a few MHz at ~100 MHz) bands of emission in radio dynamical spectra. The observed frequency in a dynamic radio spectrum corresponds to a certain height in the corona and the frequency drift is related to the velocity v_S of the shock in the direction of the density gradient. As the disturbance moves away from the active region, it will produce a shock wherever its speed exceeds the characteristic speed of the ambient medium, the fast mode magnetosonic speed $v_F = \sqrt{v_A^2 + c_S^2}$, where $v_A = B/\sqrt{4\pi n \mu m_p}$ and $c_S = \sqrt{\gamma k_B T/\mu m_p}$ is the sound speed. Here m_p is the proton mass, $\gamma = 5/3$ is the ratio of the specific heats, k_B is the Boltzmann's constant, T is the temperature, and the electron number density n_e is related to the full particle number density n by $n \sim 1.92 n_e$ for a mean molecular weight $\mu = 0.6$ (Priest 1982). If the density profile of the region over which the shock propagates is known by means of some observational diagnostic tool, an upper limit to the local characteristic speed can be set for each event by requiring $v_S > v_F$, where v_S is the speed of the shock front. By assuming radial propagation and given an estimate of the temperature, an

Send offprint requests to: S. Mancuso,
e-mail: mancuso@to.astro.it

Table 1. Spectral lines observed.

λ_{ID} (Å)	Identification	log $T_{\rm m}$
1031.91	O VI $2s\,^2S_{1/2} - 2p\,^2P_{3/2}$	5.5
1037.61	O VI $2s\,^2S_{1/2} - 2p\,^2P_{1/2}$	5.5
1215.67	Lyα	4.1

upper limit to the magnetic field strength and a lower limit to the plasma β can be finally derived from the above inequality.

Ultraviolet coronal observations can provide the required diagnostic tool needed for estimating the coronal electron plasma density along the region of propagation of the shock. The UltraViolet Coronagraph Spectrometer (UVCS) telescope aboard the Solar and Heliospheric Observatory (SOHO) spacecraft and the metric band accessible to ground-based radio spectrographs have overlapping observations for several years and probe roughly the same region of the solar corona. The metric spectral domain corresponds in fact to plasma frequencies at heights that are within the inner field of view of the UVCS instrument. This was confirmed on two known occasions when shock waves associated with Coronal Mass Ejections (CMEs) crossed the UVCS slit at the same time that type II radio emission was observed (Raymond et al. 2000; Mancuso et al. 2002). These two observations also showed that the implicit assumption that the type II emission comes from the shock in the streamer, assumption that will be used in the rest of the paper, is supported observationally. Those studies also compared the shock speed inferred from the type II frequency drift rate and standard models of the average coronal density with the speeds inferred from LASCO. The speeds inferred from the type II drift rates were in error by as much as 50%, probably as a result of differences between the actual density structure and the average models. In this paper, UVCS data were used to infer the background pre-shock coronal density profiles in which the disturbances propagate, in order to derive the shock speeds and set upper limits to the local Alfvén speed. 37 shocks were analysed in 1999 during the rise phase of cycle 22. Our major objective is to identify a definite upper limit to the coronal Alfvén speed above the active regions associated to each event in order to set firm limits to the magnetic field and plasma β in the middle corona.

In Sect. 2, a brief description of the UVCS instrument and details of the ultraviolet and radio observations are given. The criteria used for data collection and analysis of the radio and ultraviolet data are presented in Sect. 3. Finally, the results are discussed in Sect. 4, and the conclusions are drawn in Sect. 5.

2. Observations

2.1. Ultraviolet observations

The UVCS telescope measures the profiles of ultraviolet emission lines in the corona along a slit, which is placed between 1.5 and 10 $R_\odot$ from Sun center (Kohl et al. 1995). Coronal spectra are acquired in two spectrometer channels: the Lyα channel, which covers the range of 1160 to 1350 Å and the O VI channel, covering the range of 940–1123 Å. Our observations utilized

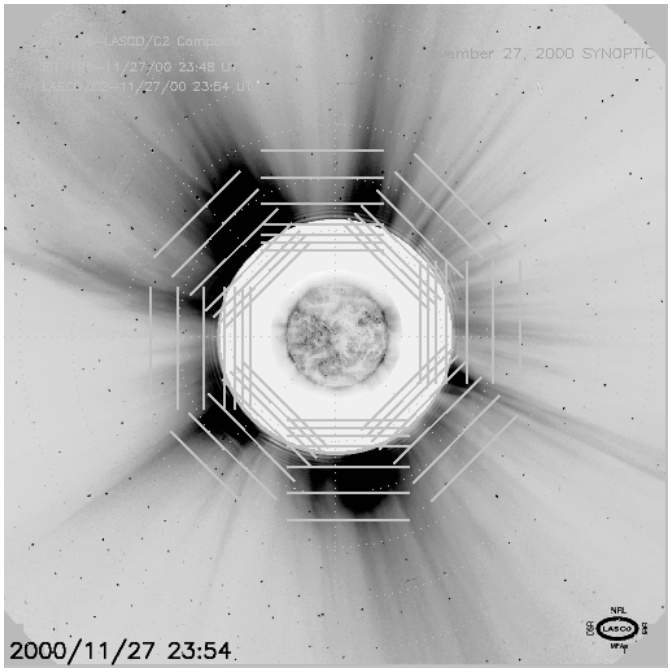

Fig. 1. A typical scheme for the UVCS synoptic program. The daily synoptic program builds up an image of the solar corona from radial scans at eight position angles. The positions of the UVCS slit relative to the solar disk are plotted over a white-light image from the LASCO coronagraph. An EIT 195 Å image obtained on the same day is also shown at the center. In this image higher intensities are shown darker.

the O VI channel that is optimized for the study of the O VI doublet 1031.91 and 1037.61 Å. A convex mirror between the grating and the detector in the O VI channel images spectral lines in the range 1160–1270 Å onto the O VI detector, allowing the detection of the redundant H I Lyα at 1215.67 Å. Table 1 lists the spectral lines observed by UVCS which were used in this work, together with their respective formation temperatures $T_{\rm m}$.

UVCS observations were obtained from the daily synoptic program which builds up an image of the corona from radial scans at eight position angles (Fig. 1). In the 1999 UVCS synoptic program, radial scans were made at six heliocentric heights (from 1.5 up to 3.5 $R_\odot$), moving the slit around the disk in steps of 45 degrees, thus providing radial profiles of the Lyα and O VI line intensities over the entire corona. A typical image built up by summing and interpolating the observations obtained at the various heights and angles in the solar corona is shown in Fig. 2 for the O VI 1032 Å line. The slit width used for synoptic observations in 1999 was 100 μm with a spatial binning scale of 21 arcsec (3 pixels) along the slit. The spectral binning was 3 pixels for the primary and 2 pixels for the redundant channel (yielding a spectral resolution of 0.2979 and 0.1830 Å respectively). In the data reduction we followed the standard techniques described in Kohl et al. (1997, 1999). The data analysis was done by using calibration routines of the new version DAS33 of the UVCS Data Analysis Software. We used DAS33 for wavelength and intensity calibration, and removal of image distortion. The uncertainties in the O VI line intensities are due to photon counting statistics, background subtraction, and radiometric calibration.

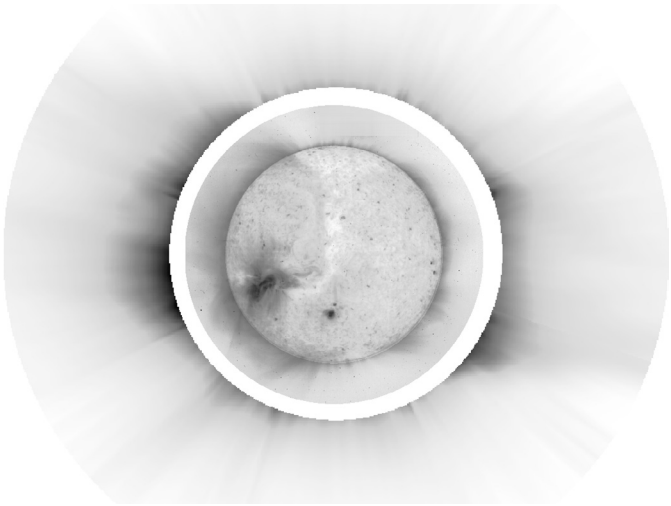

Fig. 2. UVCS 1032 Å and EIT 284 Å composite image of the corona. The image is in two parts separated by a white ring that covers a region that is not observed by either instrument. The external part (from 1.5 to 3.0 $R_{\odot}$) is an image built by the daily UVCS synoptic program from radial scans at eight position angles. In this image higher intensities are shown darker.

2.2. Radio observations

The metric type II radio bursts that were used for our study period were collected by examining the Solar Geophysical Data (SGD) bulletins published by NOAA, U.S. Department of Commerce. These bursts were observed by ground-based radio telescopes at various observatories from around the world (Learmonth, San Vito, Palehua, Culgoora, Potsdam, Hiraiso, Izmiran, and Bruny Island Observatories). Out of all the metric type II radio bursts observed during the period between March and December 1999, we selected 37 events associated to flares that occurred close to the east- or west-limb and for which we could extract information on the density profiles of the streamers above the associated active regions. Since synoptic UVCS observations were made almost daily during 1999, we were generally able to evaluate the electron density profiles of the streamers above active regions associated with the radio bursts just a few hours before the shock passage.

2.3. Auxiliary observations

Type II bursts are often associated with soft X-rays (SXR) flares (Vršnak et al. 2001). In order to associate each type II radio burst with a SXR flare, we used temporal, positional, and brightness information from the SGD reports. The flare information was used to infer the origin of the shocks over the solar surface and consequently to select the streamers above the active regions associated to the radio bursts over which the density profiles were supposed to be estimated via UV diagnostics. In addition, we used the daily movies of EUV 195 Å images obtained by the Extreme-ultraviolet Imaging Telescope (EIT) on SOHO (Delaboudinière et al. 1995) to verify the flare location over the solar surface.

Finally, it should be mentioned that most of these events were associated with CME limb events that occurred at about the same time as the bursts and above the location of the associated flares that were observed in white light with the Large Angle Spectrometric Coronagraph (LASCO; Brueckner et al. 1995) onboard SOHO. The relationship between shocks and CMEs has been already studied (Classen & Aurass 2002 and reference therein) and will not be discussed further in this paper. The analysis of a subset of the data collected here will be presented in a next paper (Mancuso et al., in preparation), that will compare the shock speeds derived from the diagnostic used in this paper with the CME speeds inferred from LASCO white light images.

3. Data collection and method of analysis

The most important parameter to be determined in our analysis of the coronal plasma properties in the middle corona is the shock speed. Calculation of the shock speed through the analysis of the drift rate of the type II radio bursts, requires the knowledge of the variation of electron density with height in the solar corona at the plasma level corresponding to the observing frequency. While the drift rate of the radio bursts can be directly determined by examining the radio dynamic spectra, the electron density is usually taken from a model. The density models refer to mean values of the electron density which have to be modified for coronal streamers and active regions by means of enhancement factors. The error on the calculation of the shock speed is therefore dependent on the functional form of the electron density-height profile being used. As already mentioned, direct observations of shocks by Raymond et al. (2000) and Mancuso et al. (2002) seem to support the view that type II emission comes from the shock near the dense streamer cores. The density diagnostics provided by ultraviolet observations can yield the required functional form of the density profile of the pre-shock plasma. In the following subsection we will present the method used to derive the electron density profiles.

3.1. Density estimate

Since the observed spectra do not include density-sensitive line ratios, we use the ratio of collisional to radiative component of the O VI 1032 Å line (Raymond et al. 1997) to estimate the plasma density. Ultraviolet lines in the lower corona form essentially by collisional excitation followed by radiative de-excitation. The intensity of collisionally excited lines depend on electron densities $n_{\rm e}$ via the line-of-sight integral of $n_{\rm e}^2$. At higher levels, and for bright enough exciting chromospheric radiation, lines form also via resonant scattering of radiation: this is the dominant process for the H I Lyα, while both components need to be considered for the O VI lines. The Lyα line is produced by resonance scattering (Gabriel et al. 1971) and is therefore subject to Doppler dimming (Hyder & Lites 1970). The two lines of the O VI resonance doublet are excited in part by collisions with free electrons, in part by transition region radiation (Kohl & Withbroe 1982), therefore their radiative components can be affected by Doppler dimming. The radiative contribution depends on the width of the coronal absorption profile, which is set by the velocity distribution of the

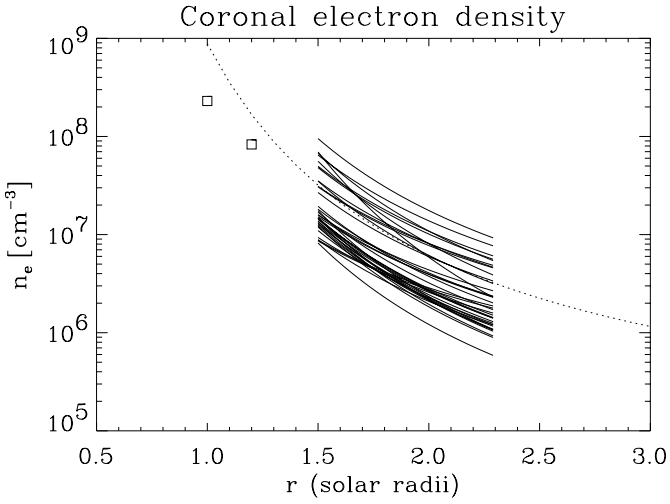

Fig. 3. Electron density estimated for the streamers above the coronal active regions associated with the type II radio bursts analyzed during the period between March and December 1999 (solid lines). The density varies over an order of magnitude. Newkirk (1961) model (dotted line), and estimates of the electron density in the inner corona from Gallagher et al. (1999) (squares) are also shown for comparison.

absorbing ions in the direction of the incoming radiation. The O VI ions, because of their larger mass and thus much narrower absorption profile, are much more sensitive to this effect than the H I atoms. The collisional and radiative components can be derived from the $I(\lambda1032)/I(\lambda1037)$ intensity ratio, which is 2 for collisional excitation

$$I_{\rm col}(\lambda1032)/I_{\rm col}(\lambda1037) = 2 \quad (1)$$

and 4 for scattering of photons from the solar disk

$$I_{\rm rad}(\lambda1032)/I_{\rm rad}(\lambda1037) = 4 \quad (2)$$

for outflow speeds lower than 100 km s^{-1} (Noci et al. 1987). The total intensity is given by $I_{\rm tot} = I_{\rm rad} + I_{\rm col}$.

For higher outflow speeds, above about 100 km s^{-1}, the Doppler dimming of the O VI 1032 Å line and the pumping of the O VI 1037 Å line by the C II 1036.34,1037.02 Å lines modify the O VI intensity ratio, and this method is no longer applicable. However, the plasma in the streamers at the heights considered in this paper can be considered approximately static. Using combined UVCS and LASCO data to determine the O VI outflow velocities as a function of height along the axis of an equatorial streamer at solar minimum, Strachan et al. (2002) found that there is no statistically significant evidence (at least at 2.3 $R_\odot$) for outflows in excess of 20 km s^{-1} anywhere within streamer cores. Velocity estimates of bulk motions seen in the solar corona by LASCO show that at all latitudes the outflow speed profiles in the corona near solar maximum have typical speeds of 50 km s^{-1} at about 2.5 $R_\odot$ (Lewis & Simnett 2002). For a nearly static plasma with negligible Doppler dimming, the coronal electron density $n_{\rm e}$ can be directly estimated from the observed ratio of the radiative and collisional components of the O VI 1032 Å line (Noci et al. 1987). The O VI intensity ratio is given by:

$$\frac{I_{\rm rad}(\lambda1032)}{I_{\rm col}(\lambda1032)} = \frac{5.75\times10^2\lambda^2\exp(\Delta E/k_{\rm B}T_{\rm e})\sqrt{T_{\rm e}}I_{\rm d}\Delta\Omega_r}{\pi g n_{\rm e}\sqrt{\Delta\lambda_{\rm cor}^2+\Delta\lambda_{\rm ex}^2}} \quad (3)$$

where λ = 1031.912 Å, $\Delta E = hc/\lambda$ is the energy difference between the levels involved in the transition, g is the Gaunt factor, $\Delta\lambda_{\rm ex}$ is the $1/e$ half width of the exciting line from the lower atmosphere, $\Delta\lambda_{\rm cor}$ is the $1/e$ half-width of the coronal absorption profile and $\Delta\Omega_r = 2\pi[1-\sqrt{1-(R_\odot/r)^2}]$ is the solid angle subtended by the solar disk at a distance r in units of solar radii. $I_{\rm d}$ is the intensity of the line integrated over the disk and was evaluated by using the O VI 1032 Å disk intensity measured near solar minimum by Zangrilli et al. (2002) with UVCS, corrected by a factor estimated from the daily Solar EUV irradiance index E10.7 for the O VI 1032 Å line from the SOLAR2000 model (Tobiska 2001). SOLAR2000 is an empirical solar irradiance specification tool for characterizing solar irradiance variability across the solar spectrum. The electron temperature $T_{\rm e}$ was estimated assuming that above the dense active regions traversed by the shocks, the density is high enough that the kinetic temperatures of the electrons and protons are the same, i.e. $T_{\rm e} = T_{\rm p}$. The proton temperature $T_{\rm p}$ was estimated from the Doppler width of the Lyα line assuming that the neutral hydrogen and the protons are coupled through charge exchange.

It is worth to emphasize that while the UVCS diagnostic is an average along the line of sight, it is dominated by any streamer near the plane of the sky. This is still an advantage compared with white light observations, for which it is necessary to assume cylindrical symmetry or else guess at the thickness of the streamer along the line of sight. Figure 3 shows (solid lines) the electron density estimated within 1.5 and 2.3 $R_\odot$ for the streamers above the coronal active regions associated with the 37 type II radio bursts between March and December 1999. In the same figure, we show the Newkirk (1961) density model (dotted line), and Gallagher et al. (1999) estimates for the inner coronal electron density above a streamer (squares). It is clear that the electron density in our sample varies over an order of magnitude in all the range. The above consideration justifies the need of adopting a specific density profile for each event in order to estimate reliable shock speeds.

3.2. Shock speed estimate

The radial velocity of a shock can be deduced from the drift rate of the associated radio signature of the drifting lanes in the dynamical spectra. In Fig. 4 we show the dynamic radio spectrum of one of the 37 type II radio bursts examined in this paper. The emission at each frequency for type II radio bursts corresponds to a specific height in the corona, with lower frequencies at greater heights. The height of the radio source can be determined from the observed coronal density profile $n_{\rm e}(r)$ via $n_{\rm e}[{\rm cm}^{-3}] = (f_{\rm pe}[{\rm Hz}]/8978)^2$. The observed negative drift is interpreted in terms of the velocity $v_{\rm S}$ with which the exciter propagates through the corona along the density gradient of a decreasing coronal density.

In the following, radial shock propagation is assumed. In the absence of spatially resolved radio spectrograph observations, it should be noted that the presence of loops and other structures of the low corona could introduce non-radial

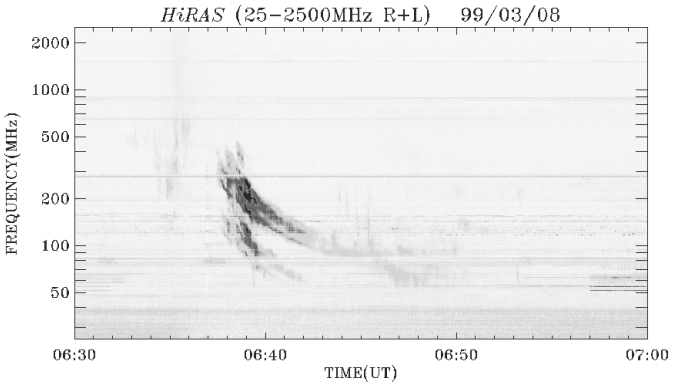

Fig. 4. The dynamic radio spectrum of one of the 37 type II radio bursts examined in this paper. The data are from the Hiraiso spectrograph in Japan and show two slowly-drifting features in the metric band. The drifting lanes are interpreted as fundamental and harmonic plasma emission from a shock moving outward through a decreasing coronal density. Courtesy of the Hiraiso Solar Terrestrial Research Center, Japan.

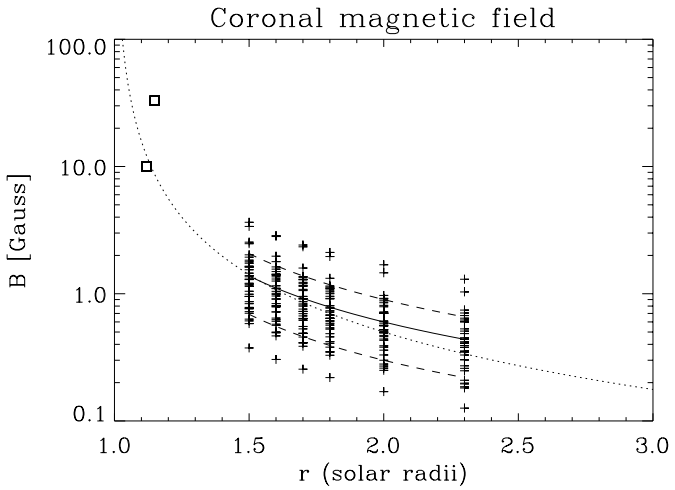

Fig. 5. Upper limits to the coronal magnetic field estimated for the streamers above the coronal active regions associated with the type II radio bursts observed between March and December 1999. The squares refer to the Lin et al. (2000) observations in the same year. The dotted line represents the Dulk & McLean (1978) model; the solid line shows our model, Eq. (6), valid between 1.5 and 2.3 $R_\odot$. The dashed lines represent the standard deviation of the data.

propagation effects. This is due to the fact that, as usually supposed, the propagation of the shock is directed along dense, low v_A regions. Nevertheless, our observations refer to heights (above 1.5 $R_\odot$) where the dense regions near the axis of streamer structures above active regions are approximately radially directed, so that problems caused by non-radial propagation should be minimized. In order to obtain plasma properties affected as little as possible by projection effects, we analyzed a set of type II radio bursts associated with east- or west- limb events. We also assumed, whenever an association between radio bursts and CMEs was found, that the shocks propagated through a medium not yet affected by the passage of the associated CMEs.

We estimated the streamer density profiles for each streamer above the coronal active regions associated with the type II radio bursts observed between March and December 1999. The density diagnostics presented in Sect. 3.1 was applied using UVCS observations taken a few hours before the shock passage above the location of the flare associated with the radio bursts under study. For convenience, the observed density profiles were fitted with the following function

$$n_e(r) = \alpha \times 10^{\rho/r} \tag{4}$$

where r is the radial distance in units of solar radii. The two parameters α and ρ are determined by fitting the observed density profile between 1.5 and 2.3 $R_\odot$. The functional form of the above model profile expressed in Eq. (4) is similar to the Newkirk (1961) density profile. The height r corresponding to the observed plasma frequency f_{pe} in the radio dynamical spectra is given by the following expression:

$$r(t) = \frac{\rho}{\log[n_e(t)/\alpha]} = \frac{\rho}{\log\left[\left(\frac{f_{pe}(t)}{8978\sqrt{\alpha}}\right)^2\right]}. \tag{5}$$

The shock speeds $v_S = \frac{dr}{dt}$ were estimated by a linear regression of the heights as a function of time, adopting the observed density profiles of the streamers above the active regions associated with each event. These estimates assume that the speed of the shock does not vary much from 1.5 to 2.3 $R_\odot$.

4. Limits to the magnetic field and plasma β in the middle corona

Given the shock speeds, calculated with the technique explained in Sect. 3.2, it is possible to derive limits to the coronal magnetic field and plasma β as follows. As the disturbance associated with an energy release moves away from the active region, it produces shocks wherever the speed of the disturbance exceeds the fast mode magnetosonic speed v_F. The speed of the shock front v_S is related to v_F by $v_S = M_F v_F$, where M_F is the magnetosonic Mach number. For a dissipative shock there is the requirement that $M_F > 1$, that is $v_F = v_S/M_F < v_S$. This requirement, given the shock speeds estimated above, allows us to obtain an upper limit to the local Alfvén speed $v_A = \sqrt{v_F^2 - c_S^2} < \sqrt{v_S^2 - c_S^2}$ above the active regions traversed by the shocks. Finally, this last inequality, due to the definition of the Alfvén speed, yields an upper limit to the coronal magnetic field just ahead of the shock front.

4.1. Upper limits to the coronal magnetic field

The estimated shock speeds were then used to set upper limits to the magnetic field (crosses in Fig. 5) above active regions using the above inequality. An average functional form of the above estimates can be represented by the following radial profile, valid between about 1.5 and 2.3 $R_\odot$:

$$B(r) \leq (0.6 \pm 0.3)(r-1)^{-1.2}\ \mathrm{G} \tag{6}$$

where r is the radial distance in units of solar radii. The above expression (solid line in Fig. 5) is consistent with the data to

within a factor of about two (the dashed lines in the same figure represent the standard deviation of the data). This model has been compared with the one obtained by Dulk & McLean (1978) using different techniques (dotted line) and valid in the wider range between 1.02 and 10 $R_\odot$. Both models are plotted in Fig. 5 over the data (crosses) derived from our analysis of the 37 radio bursts. The difference between the two models is certainly within the error and could also be due to the fact that the two sets of observations refer not only to different solar cycles, but also to different periods during a solar cycle. For completeness, we also plot in the same figure two estimates (squares) of the inner coronal magnetic field by Lin et al. (2000) obtained in the same year from observations of the longitudinal Zeeman effect.

Finally, we mention that the density derived from the type II frequency is probably the pre-shock value, but might include some compression (Mann et al. 1995). The shock compression however is small, so that M_F should not be far above unity and B should be fairly close to the upper limit found in this paper.

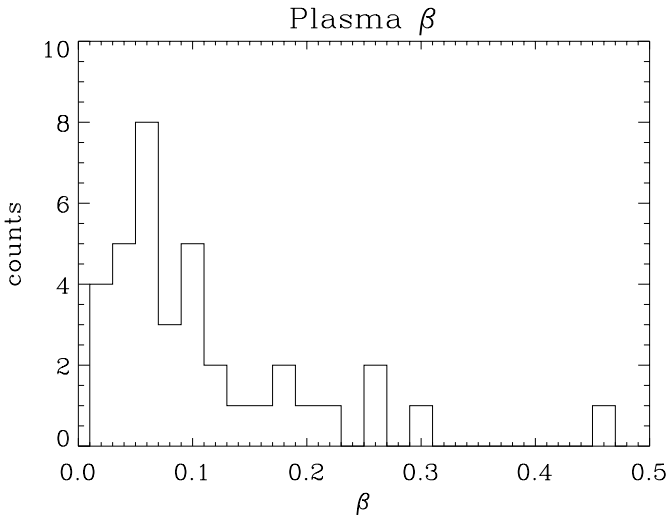

Fig. 6. Histogram of the lower limits to the average plasma β around 1.9 $R_\odot$ estimated for the streamers above the coronal active regions associated with the type II radio bursts observed during the period between March and December 1999.

4.2. Lower limits to the coronal plasma β

The lack of accurate density profiles in studies that analyze the plasma properties of the corona, also prevents the knowledge of the plasma β. The plasma β is defined by the ratio of the kinetic pressure to the magnetic one, i.e. it is related to the Alfvén and sound speed by $\beta = 8\pi n k_B T/B^2 = 2c_S^2/\gamma v_A^2$. This ratio is often assumed to be much smaller than one in the intermediate corona, although this assumption is probably not completely justified by Yohkoh/SXT observations of low cusps above active regions and MHD modelling (Suess et al. 1999; Gary 2001). Li et al. (1998) found $\beta \sim 1$ in a streamer from UV data, based on the measured gas pressure and an extrapolated potential magnetic field.

The capability of the density diagnostics provided by the UVCS instrument allows us to draw conclusions on the coronal plasma β between 1.5 and 2.3 $R_\odot$. The information extracted from our analysis is summarized in the histogram presented in Fig. 6. In this figure we show that a lower limit to the average plasma β around 1.9 $R_\odot$ estimated for the streamers above the coronal active regions associated with the type II radio bursts observed during the period between March and December 1999 can be estimated around 0.3. This lower limit for β does not conflict with the Suess et al. (1999) and Gary (2001) models.

5. Summary and conclusions

We showed that the combined analysis of radio and extreme ultraviolet spectral signatures can represent a powerful complementary tool to obtain important information about properties of the solar coronal plasma. We derived upper limits to the coronal Alfvén speed above active regions by analyzing 37 type II radio bursts observed in 1999 by ground-based radio spectrographs in conjunction with the UVCS synoptic program of monitoring of the extended solar corona. The coronal Alfvén speed upper limits were obtained by imposing the requirement that the shock speed must be greater than the local magnetosonic speed. Derivation of the shock speeds requires previous knowledge of the density profile of the coronal structures through which the shocks propagate. Instead of using generally accepted average coronal models above active regions, we estimated the density profiles of the pre-shock plasma over each active region a few hours before the passage of the shock by using the diagnostic provided by UVCS observations of the O VI doublet line intensities. We showed that the coronal electron densities varied as much as an order of magnitude above different active regions in 1999 and that therefore a single model for the coronal electron density above active regions can be misleading and unappropriate for an accurate derivation of the shock speeds.

By estimating an upper limit to the coronal Alfvén speed above each active region traversed by the shocks, we were able to set firm upper limits to the magnetic field strength and lower limits to the plasma β in the middle corona. Our main result, expressed by Eq. (6), is consistent with previous estimates of the coronal magnetic field by Dulk & Mc Lean (1978), while the plasma β estimates for the same streamers do not conflict with the Suess et al. (1999) and Gary (2001) models that require $\beta \sim 1$.

A major uncertainty in our analysis is the lack on spatial information about the effective propagation direction of each shock, that could be different from the radial. Our estimate of the shock speeds (and consequently the upper limits to the coronal Alfvén speed) would be somewhat affected in an unpredictable way by non-radial propagation effects.

Acknowledgements. The authors would like to thank the referee for his/her valuable comments and suggestions. We are also grateful to the SOHO/EIT, SOHO/LASCO and CRL (Japan) consortia for the provision of supporting images. SOHO is a project of international cooperation between ESA and NASA. The E10.7 daily index was developed by the Space Environment Technologies (SET) SpaceWx Division and is provided to NOAA/SEC through a Cooperative Research and Development Agreement (CRADA).

References

Brueckner, G. E., Howard, R. A., Koomen, M. J., et al. 1995, Sol. Phys., 162, 357

Classen, H. T., & Aurass, H. 2002, A&A, 384, 1098

Delaboudinière, J.-P., Artzner, G. E., Brunaud, J., et al. 1995, Sol. Phys., 162, 291

Dulk, G. A., & McLean, D. J. 1978, Sol. Phys., 57, 279

Gabriel, A. H., Garton, W. R. S., Goldberg, L., et al. 1971, ApJ, 169, 595

Gallagher, P. T., Mathioudakis, M., Keenan, F. P., Phillips, K. J. H., & Tsinganos, K. 1999, ApJ, 524, L133

Gary, G. A. 2001, Sol. Phys., 203, 71

Hyder, C. L., & Lites, B. W. 1970, Sol. Phys., 14, 147

Kohl, J. L., & Withbroe, G. L. 1982, ApJ, 256, 263

Kohl, J. L., Esser, R., Gardner, L. D., et al. 1995, Sol. Phys., 162, 313

Kohl, J. L., Noci, G., Antonucci, E., et al. 1997, Sol. Phys., 175, 613

Kohl, J. L., Esser, R., Cranmer, S. R., et al. 1999, ApJ, 510, L59

Lewis, D. J., & Simnett, G. M. 2002, MNRAS, 333, 969

Li, J., Raymond, J. C., Acton, L. W., et al. 1998, ApJ, 506, 431

Lin, H., Penn, M. J., & Tomczyk, S. 2000, ApJ, 541, L83

Mancuso, S., & Spangler, S. R. 1999, ApJ, 525, 195

Mancuso, S., & Spangler, S. R. 2000, ApJ, 539, 480

Mancuso, S., Raymond, J. C., Kohl, J., et al. 2002, A&A, 383, 267

Mann, G., Classen, T., & Aurass, H. 1995, A&A, 295, 775

Newkirk, G. A. 1961, ApJ, 133, 983

Noci, G., Kohl, J. L., & Withbroe, G. L. 1987, ApJ, 315, 706

Priest, E. R. 1982, Solar Magnetohydrodynamics (Dordrecht: Reidel)

Raymond, J. C., Kohl, J. L., Noci, G., et al. 1997, Sol. Phys., 175, 645

Raymond, J. C., Thompson, B. J., St. Cyr, O. C., et al. 2000, Geophys. Res. Lett., 27, 1439

Spangler, S. R., & Mancuso, S. 2000, ApJ, 530, 491

Strachan, L., Suleiman, R., Panasyuk, A. V., Biesecker, D. A., & Kohl, J. L. 2002, ApJ, 571, 1008

Suess, S. T., Gary, G. A., & Nerney, S. F. 1999, in Solar Wind Nine, ed. S. R. Habbal, R. Esser, J. V. Hollweg, & P. A. Isenberg (New York: AIP), AIP Conf. Proc., 471, 247

Tobiska, W. K. 2001, J. Geophys. Res., 106, 29969

Vršnak, B., Magdalenić, J., & Aurass, H. 2001, Sol. Phys., 202, 319

Zangrilli, L., Poletto, G., Nicolosi, P., Noci, G., & Romoli, M. 2001, ApJ, 574, 477